THE ASTROPHYSICAL JOURNAL, 452:145–155, 1995 October 10

GAMMA-RAY BURST PRECURSOR ACTIVITY AS OBSERVED WITH BATSE

THOMAS M. KOSHUT,[1,2] CHRYSSA KOUVELIOTOU,[2,3] WILLIAM S. PACIESAS,[1,2]
JAN VAN PARADIJS,[1,4] GEOFFREY N. PENDLETON,[1,2] MICHAEL S. BRIGGS,[1,2]
GERALD J. FISHMAN,[5] AND CHARLES A. MEEGAN[5]
Received 1995 February 27; accepted 1995 April 18

ABSTRACT

Gamma-ray burst time histories often consist of multiple episodes of emission with the count rate dropping to the background level between adjacent episodes. We define precursor activity as any case in which the first episode (referred to as the precursor episode) has a lower peak intensity than that of the remaining emission (referred to as the main episode) and is separated from the remaining burst emission by a background interval that is at least as long as the remaining emission. We find that ~3% of the bursts observed with the Burst and Transient Source Experiment (BATSE) on *Compton Gamma Ray Observatory* (*CGRO*) satisfy this definition. We present the results of a study of the properties of these events. The spatial distribution of these sources is consistent with that of the larger set of all BATSE gamma-ray bursts: inhomogeneous and isotropic. A correlation between the duration of the precursor emission and the duration of the main episode emission is observed at about the 3 σ confidence level. We find no meaningful significant correlations between or among any of the other characteristics of the precursor or main episode emission. It appears that the characteristics of the main episode emission are independent of the existence of the precursor emission.

Subject heading: gamma rays: bursts

1. INTRODUCTION

Gamma-ray burst time histories often show multiple episodes of emission, separated by background intervals of variable durations. We have studied those multiple episode bursts that exhibit what we classify as precursor activity. A precursor is usually thought of as something that precedes or announces something to come. Gamma-ray burst precursor activity, if it exists, may provide constraints on various burst models. It is possible, for instance, that the occurrence of a precursor event indicates an impending main episode. This may be brought about through either of two scenarios: the first may be thought of as a sympathetic process in which the precursor is distinct yet triggers the main episode. In the other scenario, the precursor and main episode are consequences of the same emission mechanism, with the time separation being due to some other intrinsic property of the source or its environment.

Additionally, precursor activity may provide insight into the physics involved in the production of gamma-ray bursts. This would be true if it were found that there is something unique to either the precursor or main episode emission properties that does not pertain to those bursts without precursors.

Early in this investigation it was recognized that a quantitative set of precursor classification criteria was necessary if the BATSE data set were to be searched for precursor activity in a systematic manner. To identify gamma-ray bursts with precursor activity, we have set four requirements that must be satisfied by any candidate event. First, the peak count rate $R_{\rm prec}$ of the first episode of emission must be less than the peak count rate $R_{\rm main}$ of the remaining main episode emission. Second, following the first episode of emission, the burst must return to a level consistent with background. Third, the duration of the background interval separating the precursor from the main episode must be at least as large as the duration (defined later in § 2) of the main episode. The second and third requirements are the means by which we distinguish precursor emission from emission that is simply the first pulse of an extended event. And finally, the locations of the first episode and the main episode must be consistent with the same position in the sky. This fourth requirement is a verification that the two emissions share the same source object. We consider the first three requirements to be rather conservative, providing a data set with rather extreme precursor properties; they may be relaxed in future studies.

2. PROCEDURE

BATSE consists of eight detector modules, each located at a corner of the *Compton Gamma Ray Observatory* (*CGRO*) spacecraft. Each detector module consists of an uncollimated Large Area Detector (LAD) and a Spectroscopy Detector (SD). For this investigation we used only data from the LADs. The onboard flight software continuously monitors the count rates observed over the energy range of ~50–300 keV for 5.5 σ excesses above background simultaneously in two or more LADs. This monitoring is done on three timescales: 64 ms, 256 ms, and 1.024 s. Once these criteria have been met on any of these timescales, a trigger is declared and burst data (with high temporal and spectral resolution for a fixed length of time) are recorded. Various data types are available for each triggered event, but in this study we used only the LAD discriminator data (DISCLA). DISCLA data consist of count rates in four energy channels with a time resolution of 1.024 s and are always available (except at times of *CGRO* telemetry gaps). The approximate energy ranges of the four energy channels are 20–50 keV, 50–100 keV, 100–300 keV, and >300 keV. Further details of BATSE instrumentation and data types can be found elsewhere (Fishman et al. 1989).

[1] Department of Physics, University of Alabama in Huntsville, Huntsville, AL 35899.
[2] Postal address: NASA/Marshall Space Flight Center ES84, Huntsville, AL 35812.
[3] Universities Space Research Association.
[4] Astronomical Institute "Anton Pannekoek," University of Amsterdam, Kruislaan, 403, 1098 SJ Amsterdam, Netherlands.
[5] NASA/Marshall Space Flight Center ES84, Huntsville, AL 35812.

2.1. *Preliminary Event Selection*

A preliminary search to identify precursor candidate events was performed. Three plots of DISCLA data from each of the eight LADs were used in this initial search. The three plots correspond to the energy ranges 25–50 keV, 50–300 keV, and >300 keV. The time resolution of these plots was 2.048 s. The data spanned the time range from 1000 s before the BATSE trigger time to 1000 s following the trigger time. These plots were searched by eye for emission that preceded the main episode, that was separated from the main episode by what appeared to be background data, and that was of lower peak intensity than the main episode. It was not required that the precursor candidate be of sufficient intensity to trigger the on-board software. We did require that the precursor and the main episode both be detected simultaneously in at least two LADs and that the ratio of their peak intensities be about the same in each of the detectors. No requirements were placed on the energy ranges in which the precursor must be observed. Up to this point, these criteria were loosely applied; those events that appeared almost to meet the criteria were included as candidates, which allowed for a more rigorous application of all precursor criteria in the detailed analysis. As a result, several of the candidate events were later excluded in the detailed analysis.

2.2. *Intensive Analysis*

In the final analysis, we used the DISCLA at their intrinsic time resolution of 1.024 s. The data were summed over each of the triggered BATSE detectors (a minimum of two detectors and a maximum of four). A background model was created for each energy channel by fitting user-defined background intervals with a second-degree polynomial and interpolating this fit across the source interval.

We subtracted the background model from the observed count rates in each energy channel. This then gave us the source count rates as a function of time in each channel. We also summed the source count rates over energies >20 keV, which gave us the total source count rates as a function of time. Using this, along with the background models summed over the same energy range, we then calculated the signal-to-noise ratio (S/N) as a function of time. We proceeded to choose two time intervals, I_p and I_m; interval I_p would be searched for significant precursor emission, and interval I_m would be searched for significant main episode emission. The start times of the precursor and the main episode were determined by finding the earliest significant signal following the start of the intervals I_p and I_m, respectively. The end times of the precursor and the main episode were determined by finding the last significant signal within the intervals I_p and I_m, respectively. In this study we defined a significant signal as either three consecutive points at least 2 σ above background, two consecutive points at least 3 σ above background, or one point at least 4 σ above background.

The durations of both the precursor (τ_{prec}) and the main episode (τ_{main}) were then defined as the differences between their respective start and end times. In addition, the separation time Δt_{det} between detectable emission was calculated as the time between the end of the precursor and the start of the main episode. The peak rates R_{prec} and R_{main} (summed over all four channels), their uncertainties, and the peak times of the precursor and the main episode were then found, as well as the separation time Δt_{pk} between the peaks of the precursor and main episode emissions. Figure 1 illustrates these parameters as applied to one of the candidate events. The background-subtracted count rates, and their uncertainties, in each of the four energy channels at the peak times were also determined. The total number of background-subtracted counts, and their uncertainties, observed in each of the four energy channels during the precursor and the main episode were also calculated.

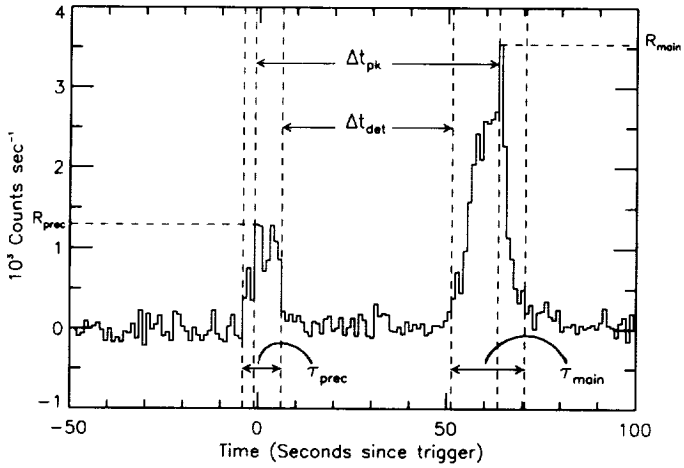

FIG. 1.—Illustration of various parameters defined in the text. Δt_{pk} is the separation time between the peak count rates of the precursor and main episode emission. Δt_{det} is the separation time between detectable emission, defined using the end time of the precursor emission and the start time of the main episode emission. τ_{prec} and τ_{main} are the durations of the precursor and main episode emissions, respectively. R_{prec} and R_{main} are the background-subtracted peak count rates, summed over the entire energy range to which the BATSE LADs are sensitive, of the precursor and main episode emissions.

The preliminary set of events was first tested using two of the four previously mentioned precursor criteria. The requirement that the peak intensity of the first episode be less than that of the main episode was satisfied by checking that the S/N at the time of peak intensity of the main episode was at least 1 σ greater than that of the precursor episode in the energy range 50–300 keV. In addition, the requirement that the separation between the precursor and the main episode be at least as large as the duration of the main episode was then satisfied using Δt_{det} and the main episode duration τ_{main}.

Next, we demanded that the burst must have returned to background following the precursor event. This was accomplished by calculating the total number of counts observed over the entire energy range during a window sliding through time. The width of the window was the smaller of 10.240 s or the duration of the precursor. Thus, the width of the window could vary from burst to burst (which allowed us to avoid a bias against precursors with durations less than some arbitrary window width) but remained constant within any single burst. The sliding window was applied to the precursor, and the interval with the largest number of total counts was selected. The window was then applied to the background interval, starting at the end of the precursor; the smallest number of counts observed in this window was recorded. We defined a return to background as the smallest number of counts in any background window being less than 5% of the largest number of counts in any precursor window.

We used a relative limit (5% of precursor counts) in our test for a return to background rather than an absolute limit. In this way we avoid introducing a distance bias into our selec-

tion criteria. As a tradeoff, we must recognize the possibility that an event with a strong precursor may clearly show significant flux during an interval that we are designating as background. This is not that costly a tradeoff when one considers that we cannot reject the existence of source emission below our detection level during any time interval for any burst. Thus, our criterion for returning to background, as defined, is not a guarantee that the source has entered a quiescent state.

A final requirement was then applied to those bursts that had qualified thus far as having precursors: the locations of the precursor and the main episode must be consistent with the same position on the sky. Locations were computed for both the precursor and the main episode emission of each event using the standard BATSE burst location software (Brock et al. 1992). None of the candidate events were eliminated by this requirement. The angle ξ between the location of the precursor and that of the main episode was calculated, and the mean value was found to be $\langle \xi \rangle = 13°$ with a standard deviation of 10°. Figure 2 shows the distribution of the offsets (in σ) of the precursor locations from the main episode locations. The largest offset was 2.7 σ.

3. RESULTS

We examined 995 BATSE bursts in the preliminary precursor search. These bursts were observed during the time interval from 1991 April 5 (*CGRO* launch) through 1994 May 29. Mostly because of telemetry gaps, 247 of these bursts had insufficient data for determining the existence of precursor activity. Of the remaining 748 bursts, 24 qualified as precursor events, which showed that ~3% of the bursts observed with BATSE exhibit precursor activity that meets the four previously mentioned requirements. Table 1 gives the BATSE trigger numbers and burst names for these 24 events. Figure 3 shows the temporal profiles for the 24 events.

3.1. *Global Characteristics*

Figure 4 shows the sky distribution of the precursor events in Galactic coordinates. Much like the larger set of all BATSE bursts (Meegan et al. 1994a), the distribution of locations for this subset of bursts is consistent with an isotropic distribution. Table 2 contains the results of the isotropy tests in various coordinate systems. The dipole moment $\langle \cos \theta \rangle$ to the Galactic center (where θ is the angle between the burst location and the Galactic center) and the quadrupole moment $\langle \sin^2 b - \frac{1}{3} \rangle$ about the Galactic plane (where b is the Galactic latitude of a burst location) are consistent with that expected for an isotropic distribution (the expected values of these two statistics for an isotropic distribution have been corrected here for the nonuniform BATSE sky exposure). The quadrupole moment $\langle \sin^2 \beta - \frac{1}{3} \rangle$ about the ecliptic plane (where β is the ecliptic latitude) is also within 1 σ of that expected for an isotropic distribution, as is the dipole moment $\langle \cos \phi \rangle$ (where ϕ is the angle between the burst and the Sun) toward the Sun (Horack et al. 1994). These two tests would enhance isotropies expected for any heliocentric model. Coordinate system–independent tests for anisotropy were also performed (Briggs 1993). The Rayleigh-Watson statistic $\mathscr{W}$, which tests for a dipole moment, and the Bingham statistic $\mathscr{B}$, which tests for a quadrupole moment, are both consistent with an isotropic sky distribution (again, corrected for the nonuniform BATSE sky exposure). We find no significant concentration of bursts toward the Galactic center, α Centauri, M31, the Large Magellanic Cloud, or the Virgo Cluster.

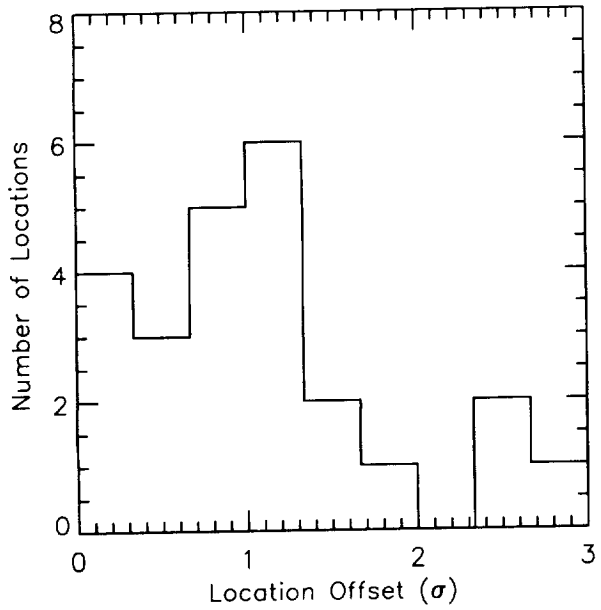

FIG. 2.—Distribution of the offsets of the precursor locations from the main episode locations.

TABLE 1

LIST OF PRECURSOR EVENTS

BATSE Trigger Number	BATSE Burst Name
211	1B 910518B
222	1B 910523
235	1B 910528
351	1B 910614B
1145	1B 911204
1192	1B 911217B
1196	1B 911219B
1656	2B 920619
1815	2B 920814
1830	2B 920816
2053	2B 921112
2110	2B 921230
2123	2B 930108
2148	2B 930127B
2160	2B 930203
2277	3B 930331B
2435	3B 930608
2451	3B 930720B
2510	3B 930902
2528	3B 930913
2614	3B 931101
2640	3B 931117
2727	3B 940101B
2862	3B 940305C

TABLE 2

STATISTICAL TESTS OF ISOTROPY

Statistic	Value Expected for Isotropy	Value Measured	Deviation from Isotropy
$\langle \cos \theta \rangle$	-0.013 ± 0.118	-0.031	$-0.2\ \sigma$
$\langle \sin^2 b - \frac{1}{3} \rangle$	-0.005 ± 0.061	-0.059	$-0.9\ \sigma$
$\langle \sin^2 \beta - \frac{1}{3} \rangle$	$0. \pm 0.061$	-0.024	$-0.4\ \sigma$
$\langle \cos \phi \rangle$	$0. \pm 0.118$	0.022	$0.2\ \sigma$
$\mathscr{W}$	3.0 ± 2.4	0.3	$-1.2\ \sigma$
$\mathscr{B}$	5.2 ± 3.2	5.3	$<0.1\ \sigma$

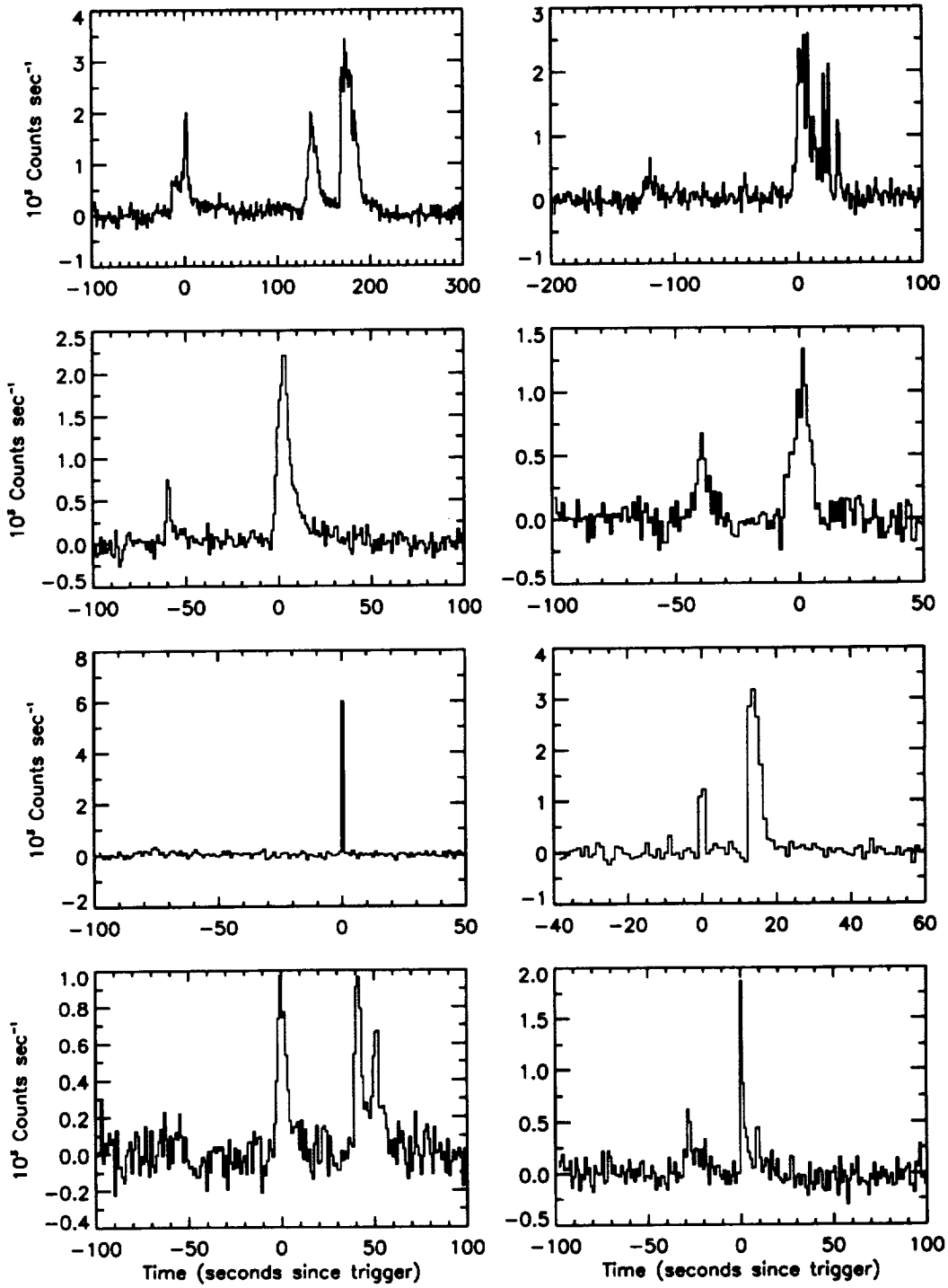

FIG. 3—*Continued*

the larger 1.024 s time bin. Thus, there is an intensity bias against the observation of short-duration (≤ 1.024 s) precursor emission. This bias is worsened by our definition of significant emission for short episodes, which requires that any precursor or main episode emission with a duration ≤ 1.024 s must exceed background by at least 4 σ (as opposed to either 2 σ or 3 σ for longer duration events).

The distributions of the peak-to-peak separation time Δt_{pk} and the separation time Δt_{det} between detectable emission are shown in Figure 6. We find that $\langle \Delta t_{det} \rangle = 90 \pm 18$ (85) s and $\langle \Delta t_{pk} \rangle = 114 \pm 22$ (104) s. This result is not surprising since it is clear from their definitions that Δt_{pk} can never be less than Δt_{det}. Additionally, we find a strong correlation between Δt_{det} and Δt_{pk} (to be discussed in more detail in § 3.2).

Note that the distribution of Δt_{det} is convolved with the distribution of τ_{main} through one of the required precursor criteria. This effect is also propagated into the distribution of Δt_{pk} through the strong correlation between Δt_{det} and Δt_{pk}

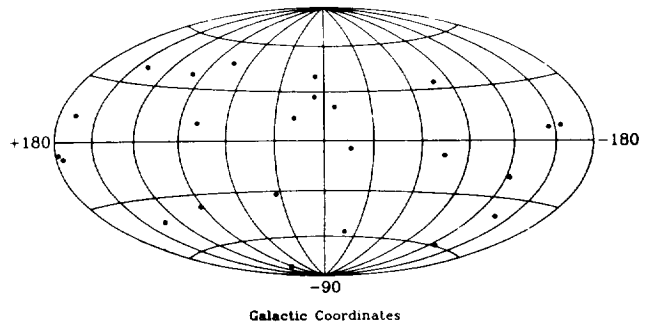

FIG. 4.—Sky distribution of the 24 precursor bursts in galactic coordinates. The distribution is consistent with isotropy in Galactic coordinates, as well as in other coordinate systems.

already mentioned. Thus, the lower limit at ~ 10 s in Figure 6 is probably an artifact of the cutoff in the distribution of τ_{main}. In addition, it is important to note that the use of data with a minimum time resolution of 1.024 s does not allow us to make any statements about the existence of precursor activity with $\Delta t \leq 1.024$ s. During the preliminary search we found several events that would almost certainly have met our four precursor criteria if we would have used data with a finer time resolution. We could not use these fine time resolution data because they are available only beginning at 2.048 s before the burst trigger time, thus not covering the precursor emission in the majority of the precursor events.

Figure 7 shows the distribution of the ratio of peak rates R_{prec}/R_{main}. Note that by our precursor criteria this ratio must always have a value less than 1. In only two of the 24 cases were the peak rates of the precursor and main episode emissions comparable. In all other cases, R_{prec} was less than 60% of R_{main}. The mean ratio is $\langle R_{prec}/R_{main} \rangle = 0.37 \pm 0.05\,(0.26)$.

We define a parameter λ_{pk}, which characterizes the position

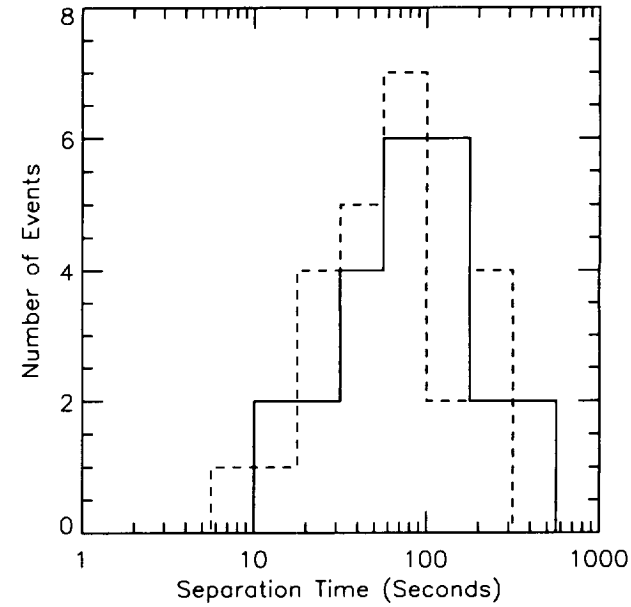

FIG. 6.—Distributions of the separation time between detectable emission Δt_{det} (*dashed curved*) and the peak-to-peak separation time Δt_{pk} (*solid curve*). The mean separation times are $\langle \Delta t_{det} \rangle = 90 \pm 18$ (25) s and $\langle \Delta t_{pk} \rangle = 114 \pm 22\,(104)$ s.

of the peak intensity within an emission episode, as

$$\lambda_{pk} \equiv \frac{\tau_r}{\tau}, \tag{1}$$

where τ_r (historically referred to as the rise time) is the time interval from the start of the emission to the peak time of the emission and τ is the duration of the emission episode. Note that the value of λ_{pk} is constrained to fall within the range

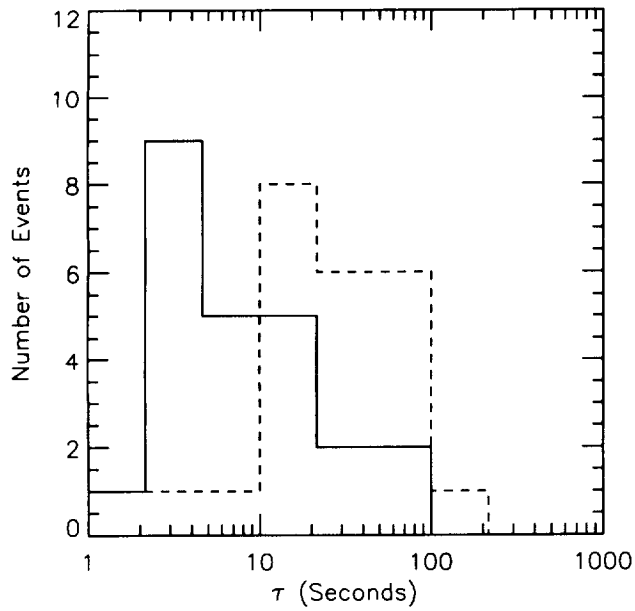

FIG. 5.—Duration distributions of the precursor emission (*solid curve*) and of the main episode emission (*dashed curve*). The mean durations are $\langle \tau_{prec} \rangle = 12.1 \pm 2.8\,(13.5)$ s and $\langle \tau_{main} \rangle = 36.2 \pm 7.5\,(36.9)$ s.

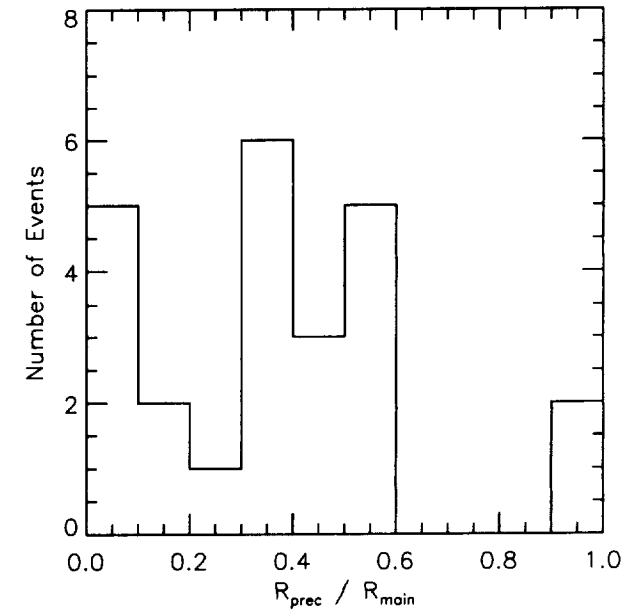

FIG. 7.—Distribution of the ratio of the precursor peak rate to the main episode peak rate. In only two cases are the peak rates of the two emissions comparable.

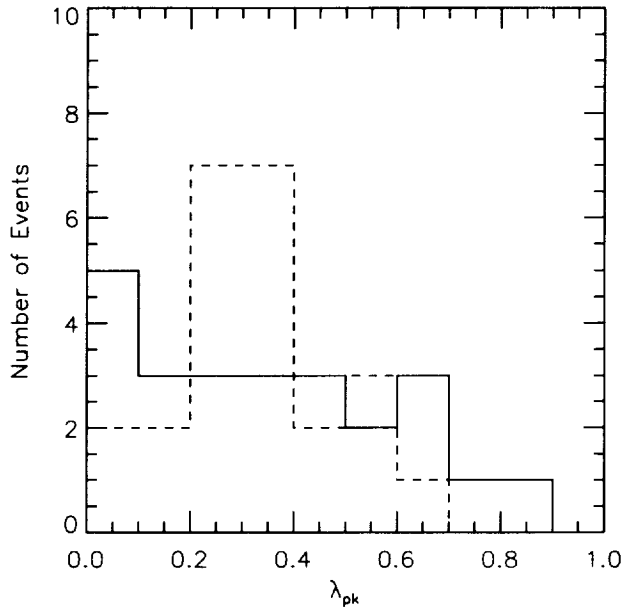

FIG. 8.—Distribution of λ_{pk}, a measure of the position of the peak emission within an emission episode, for both the precursor emission (*dashed curve*) and the main episode emission (*solid curve*).

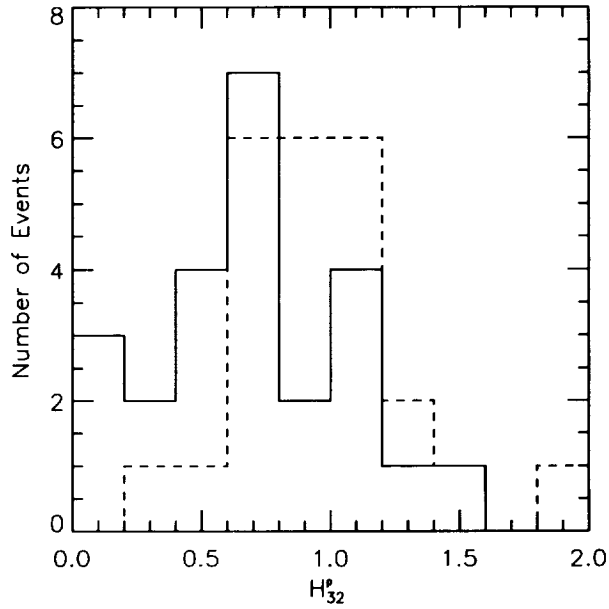

FIG. 9.—Distribution of the hardness ratio H^p_{32} for the precursor emission (*solid curve*) and for the main episode emission (*dashed curve*).

$0 < \lambda_{pk} < 1$. Figure 8 shows the distribution of this parameter for both the precursor emission and the main episode emission. For the precursor emission, we measure $\langle \lambda_{pk} \rangle = 0.32 \pm 0.04$ (0.17). For the main episode emission, we find that $\langle \lambda_{pk} \rangle = 0.35 \pm 0.05$ (0.25). Thus, for both the precursor and main episodes the peak intensity of the emission tends, on average, to occur early in the emission episode. However, the KS test does not allow us to reject the hypothesis that the two distributions are drawn from the same parent distribution, with $P(d, N) = 0.387$.

To gain greater insight into the precursor phenomenology, we also examined the spectral characteristics of the precursor events. To accomplish this, we define two types of hardness ratios. Hardness ratios of the first type are defined as

$$H^p_{ij} \equiv \frac{R_i}{R_j}, \tag{2}$$

where R_i is the count rate in energy channel i at the time of the peak rate (with the peak rate determined from the time history summed over the entire LAD energy range). Hardness ratios of the second type are defined as

$$H^t_{ij} \equiv \frac{C_i}{C_j}, \tag{3}$$

where C_i is the total counts in energy channel i, integrated over the duration of the emission. When one compares hardness ratios, it is important not to use hardness ratios defined over different energy ranges.

Figure 9 shows the distributions of H^p_{32} for both the precursor and main episode emissions. We find that $\langle H^p_{32} \rangle = 0.70 \pm 0.08$ (0.38) for the precursor emission while $\langle H^p_{32} \rangle = 0.93 \pm 0.07$ (0.33) for the main episode emission. This shows a weak tendency for precursor peak emission to be softer, on average, than main episode peak emission. However, there are several individual cases in which the precursor peak emission is harder than the average main episode peak emission. The KS test does not allow rejection of the hypothesis that the two distributions are drawn from the same parent distribution, with a KS probability of $P(d, N) = 0.275$. Figure 10 shows the distributions of H^t_{32} for both the precursor and main episode emission. We find that $\langle H^t_{32} \rangle = 0.80 \pm 0.08$ (0.38) for the precursor emission while $\langle H^t_{32} \rangle = 0.84 \pm 0.06$ (0.29) for the main episode emission. Thus, though precursor peak emission tends to be somewhat softer than main episode peak emission, there is no evidence that this holds true over the entire event. This may be a result of spectral evolution during the precursor emission, the main episode emission, or both. Again, in Figure 10 there are clear examples of precursor emission that is harder than the average main episode emission. The KS test does not allow rejection of the hypothesis that the two distributions were drawn from the same parent distribution, with a KS probability of $P(d, N) = 0.77$.

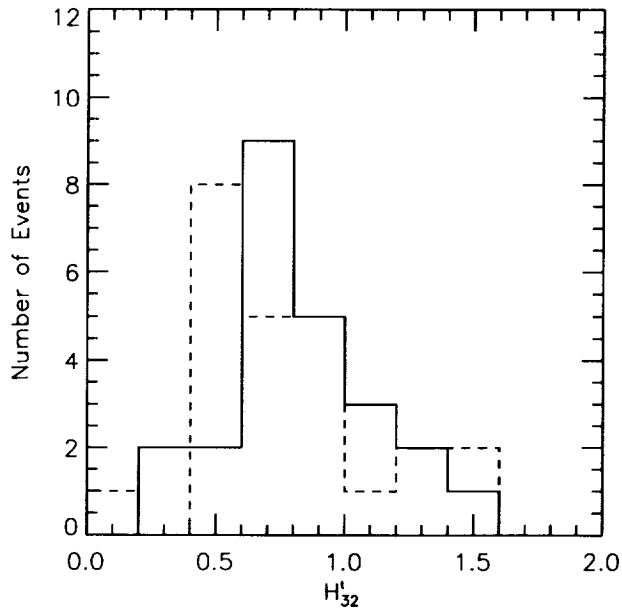

FIG. 10.—Distribution of the hardness ratio H^t_{32} for the precursor emission (*dashed curve*) and for the main episode emission (*solid curve*).

The distributions of H^p_{21} for the precursor and main episode are essentially indistinguishable. We find that $\langle H^p_{21} \rangle = 1.33 \pm 0.12$ (0.59) for the precursor emission, while $\langle H^p_{21} \rangle = 1.45 \pm 0.10$ (0.48) for the main episode emission. The distributions of H^t_{21} are similar. We find that $\langle H^t_{21} \rangle = 1.10 \pm 0.07$ (0.35) for the precursor emission while $\langle H^t_{21} \rangle = 1.18 \pm 0.05$ (0.25) for the main episode emission. Again, the KS test cannot reject the hypothesis that the precursor and main episode emission distributions are drawn from the same parent distribution.

Hardness ratios may possibly be used to compare the precursor's surrounding burst environment or production mechanism with that of the average gamma-ray burst source. The parameter that we use to do this is a ratio of H^t_{32} for the precursor emission to H^t_{32} for the main episode emission. The distribution of this ratio is shown in Figure 11*a* for our sample of 24 precursor events. The mean value of this ratio is calculated to be 1.02 ± 0.10 (0.50). If the average precursor's surrounding burst environment or production mechanism is similar to that of the average burst, then we would expect the disribution shown in Figure 11*a* to be consistent with the distribution of the same ratio for all observed BATSE bursts, if we use randomly selected burst pairs to calculate the ratio. The hardness ratio H^t_{32} has been calculated for each BATSE burst (Kouveliotou et al. 1993) using the total counts observed in each channel during the T_{90} time interval (the time interval during which the integrated counts above background increases from 5% to 95%). We selected burst pairs in chronological order from the BATSE 2B Gamma-Ray Burst Catalog (Meegan et al. 1994b), and we allowed each burst to be used in only one pair. After we eliminate the 24 precursor events from this sample, this provided 207 pairs. We then calculated the ratio of H^t_{32} for each of the 207 pairs. This distribution is shown in Figure 11*b*. We find that the mean value of this ratio for the 207 events is 1.30 ± 0.09 (1.29), consistent with the value given above for the precursor events. The KS test does not allow us to reject the hypothesis that the two distributions are drawn from the same parent distribution, with $P(d, N) = 0.57$. Thus, with respect to these hardness ratios the relationship between the precursor and main episode emission, which we know to be from the same source, is the same as that between two emission episodes from completely different sources. This may be an indication that neither the burst production mechanism nor the precursor emission site environment is distinct from those of an average gamma-ray burst.

3.2. *Correlations between Emission Characteristics*

We also searched for three types of correlations between the various parameters. The first type is a correlation between a precursor emission characteristic and a main episode emission characteristic. Any such correlation may indicate the presence of a single burst production mechanism and would provide strong constraints on various burst models. The second is a correlation between two characteristics of the same emission episode; this correlation may not prove very useful in distinguishing between distinct precursor and main episode production mechanisms but might provide insight into the mechanism producing that emission episode. The third correlation is between a characteristic of an emission episode and a global event parameter such as a separation time Δt.

The statistical tool we used to quantify the degree of correlation between two parameters was the Spearman rank-order correlation coefficient r_s (Press et al. 1986, p. 634). The Spearman correlation coefficient has the advantage that, unlike the more common linear correlation coefficient, no assumptions need be made about the parent population from which the data are sampled in order to assess the significance of the result.

We first investigated the dependence of the strength of the main episode emission on the strength of the precursor emission. The strength of the event can be characterized by either peak flux or total fluence of the emission. We used the peak count rate as a measure of the peak flux of the emission and the total counts as a measure of the fluence. We found no evidence for correlation between the strength of the main episode and

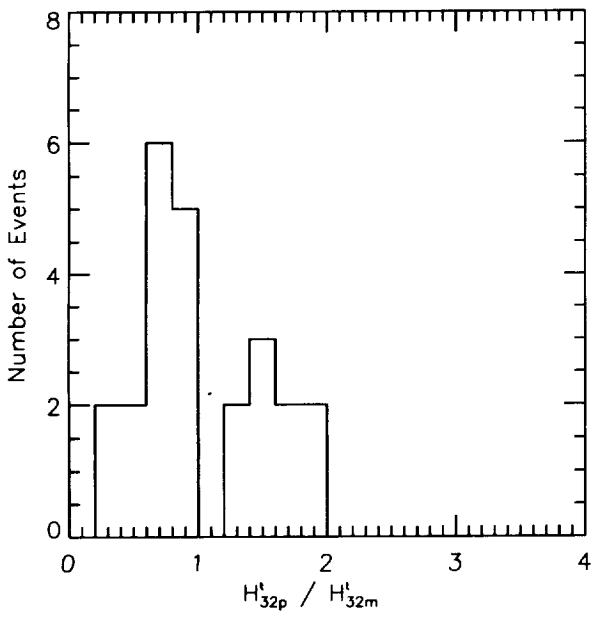

FIG. 11*a*

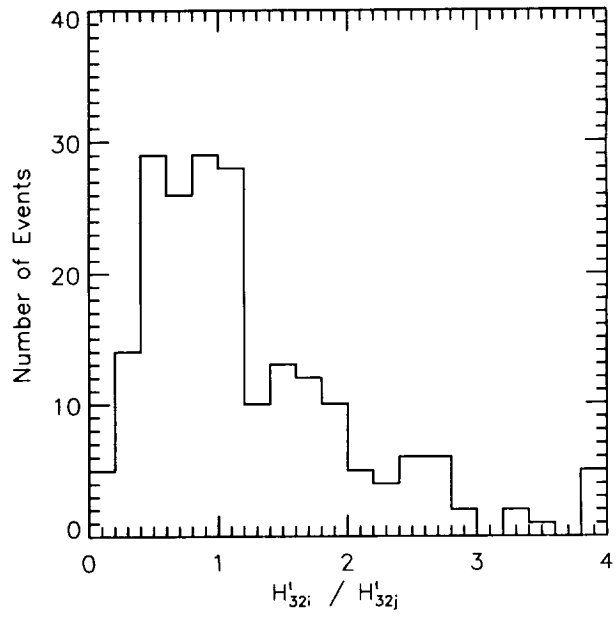

FIG. 11*b*

FIG. 11.—(*a*) Distribution of the ratio of H^t_{32} for the precursor emission to H^t_{32} for the main episode emission. The total number of events is 24. (*b*) Distribution of the ratio of H^t_{32} for 207 burst pairs, paired in chronological order, taken from the larger data set of the BATSE 2B Gamma-Ray Burst Catalog.

the strength of the precursor emission using either peak rate or total counts.

Next we examined the dependence of the duration of the main episode emission on the duration of the precursor emission. Figure 12 shows a plot of the duration of the main episode emission versus that of the precursor emission. We see that there is a positive correlation, with $r_s = 0.59$, with the probability of chance correlation $P(r_s, N) = 2.4 \times 10^{-3}$.

In a similar way we looked for various correlations between the other properties of the precursor and the main episode emissions. These properties include duration, peak rate (summed over the entire LAD energy range), total counts (summed over the entire LAD energy range), the previously defined hardness ratios, and the peak position parameter λ_{pk}. In no case did we find evidence for a significance correlation; in all cases, the data were consistent with no correlation between the quantities. Therefore, having found no physically meaningful significant correlations between the various characteristics of the precursor and main episode emissions, we conclude that we find no evidence that the characteristics of the main episode emission are dependent upon the existence of the precursor emission.

We next proceeded to search for significant correlations among the characteristics of either emission. As would be expected, we found significant positive correlations between τ_{prec} and total precursor counts, between the precursor peak rate (summed over the four energy channels) and the total precursor counts, and between τ_{main} and the total main episode counts. In no other case did we find evidence for a significant correlation among the characteristics of either emission; in all cases, the data were consistent with no correlation between the quantities.

We did observe a significant strong correlation between Δt_{det} and Δt_{pk}. This correlation is simply a consequence of the definitions of Δt_{det} and Δt_{pk}, the fact that on average the $\tau_{prec} < \tau_{main}$, and the previously mentioned observation that the peak intensity of the main episode tends to occur early in the emission episode. In addition, we observed significant correlations between Δt_{pk} and τ_{main} as well as between Δt_{det} and τ_{main}. However, both of these correlations are also artifacts of our precursor criteria. We found no evidence for correlations between either Δt_{det} or Δt_{pk} and any of the other precursor or main episode emission characteristics.

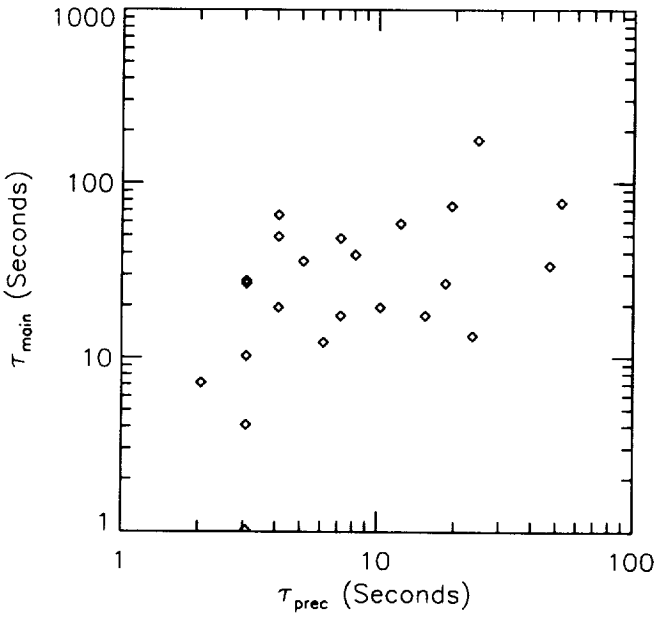

FIG. 12.—Plot of precursor duration τ_{prec} vs. main episode duration τ_{main}. We find $r_s = 0.59$ and $P(r_s, N) = 2.4 \times 10^{-3}$.

The phenomenology of X-ray bursts (Lewin, van Paradijs, & Taam 1993) was classified by the recognition of two types of burst with very different spectral and recurrence properties. For the one type of X-ray burst the fluence in a burst and the time until the next burst are correlated. These (so-called type II) bursts therefore show a relaxation oscillator behavior. For the other type of burst (type I bursts) there is a global correlation between the burst strength and the time since the previous burst (indicative of an accumulation of fuel). The observation of both types of burst from one peculiar source (the "Rapid Burster") led to the recognition that the type I X-ray bursts are caused by thermonuclear flashes on the surface of a neutron star and the type II bursts by an accretion instability (Hoffman, Marshall, & Lewin 1978).

We searched our data set for similar correlations within gamma-ray burst profiles that show precursor activity. We certainly do not imply that X-ray burst models are applicable to gamma-ray bursts as well; however, correlations of these types would provide constraints on any gamma-ray burst model. We examined how the relative strength of the precursor and main episode emissions depended upon the separation time between the two emissions. To characterize the relative strength of the events, we used two ratios: the ratio of the total precursor counts to the total main episode counts and the ratio of the precursor peak rate R_{prec} to the main episode peak rate R_{main}. By using ratios, we were able to eliminate the distance dependence from our strength parameters. As before we used Δt_{det} and Δt_{pk} as measures of separation time. Figure 13 shows the ratio of the total precursor counts to the total main episode counts versus Δt_{det}. We find no evidence of correlation between the two quantities. However, it can be seen from Figure 13 that there seems to be a tendency for the energy released in gamma rays during the precursor to be a smaller portion of the total gamma-ray energy budget for large separation times. The tendency remains when Δt_{pk} is used as the measure of separation time (as would be expected because of the strong correlation between Δt_{det} and Δt_{pk} discussed in § 3.2). No evidence was found for any correlation between R_{prec}/R_{main} and either of the measures of the separation time.

4. DISCUSSION

Earlier work on gamma-ray burst precursor emission was done by Murakami et al. (1991, 1992), Lochner (1992), Horack & Emslie (1994), and Yoshida & Murakami (1994). Both Murakami et al. (1991) and Yoshida & Murakami (1994) reported on soft X-ray precursor emission prior to the onset of the gamma-ray emission. Their work differs from our study in two fundamental ways. First, their precursor emission does not return to background before the onset of the gamma rays; thus, one may think of their observations as extreme cases of spectral evolution within a single emission episode. Second, many of their precursor data were obtained at energies below the sensitive range of the detectors used herein.

In addition to the precursor emission just discussed, Murakami et al. (1992) report that *Ginga* observed at least three precursor events in which there was a clear separation of the precursor event from the onset of the gamma-ray emission. They found that the spectra of the precursor events were extremely soft when compared with the main burst emission.

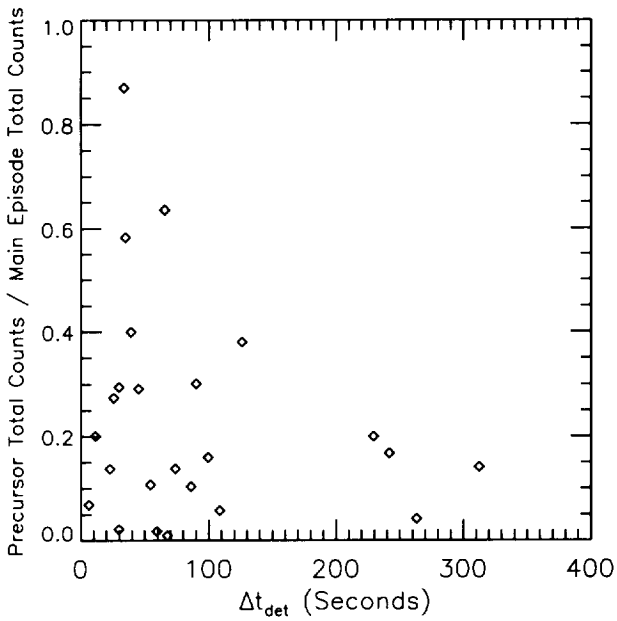

FIG. 13.—Plot of the ratio of the precursor total counts to the main episode total counts vs. the separation time Δt_{det}. We find $r_s = -0.13$ and $P(r_s, N) = 0.55$.

When we used hardness ratios, we found that there was a tendency for the precursor peak emission to be softer, on average, than the main episode peak emission, but we found no evidence that this held true over the entire event. It is interesting to note that there are several cases in our sample of events in which the precursor emission is harder than the main episode emission.

Lochner (1992) studied the relationships between successive episodes in multiple episode bursts observed with the *Pioneer Venus Orbiter* (*PVO*) gamma-ray burst detector. Unlike the work presented here, which divides a burst into its precursor emission and the remaining emission, he allowed for multiple pairs of successive events within a single burst. His selection criteria were more relaxed in that they did not impose requirements on the relative intensities of the two successive episodes or on the time interval separating any two emission episodes. In addition, his data set was only a sample of multiple event bursts and did not result from a systematic search through the entire *PVO* database.

Lochner reported a strong correlation [$r_s = 0.73$, $P(r_s, N) = 3.2 \times 10^{-8}$] between the duration of an event and the duration of the subsequent event. We note that our results (see § 3.2) are consistent with this correlation. He also reported a moderately strong correlation [$r_s = 0.48$, $P(r_s, N) = 3.1 \times 10^{-4}$] between the hardness of an event and the hardness of the following event. We found no evidence for this correlation, but this may be due to either the small number of events in our sample or to the different energy ranges used in the calculation of the hardness ratios (Lochner defines his hardness ratio H as the ratio of the total counts in the energy range 200–2000 keV to the total counts in the energy range 100–200 keV).

Horack & Emslie (1994) used the BATSE occultation technique (Harmon et al. 1991) to search for long-term low-level emission from the positions of 70 intense bursts. They found no evidence that those bursts emit preburst emission at a detection level exceeding $\sim 5 \times 10^{-9}$ ergs cm^{-2} s^{-1} on timescales of ~ 1 hr or longer. However, they note that because of the nature of the occultation measurement process (each source is measured over a short time interval twice during each 90 minute spacecraft orbit), they cannot place detection limits on objects that burst over timescales of minutes or seconds. The precursor emissions reported on here occur on these shorter timescales.

5. CONCLUSIONS

We find that $\sim 3\%$ of the cosmic gamma-ray bursts observed with BATSE exhibit precursor activity, as defined by us here. The distribution of these events on the sky is consistent with isotropy, using both coordinate system–dependent and coordinate system–independent tests. When we use the V/V_{max} test, we find that their spatial distribution is consistent with inhomogeneity. When we use hardness ratios, we find no evidence that the circumstances in which the precursor emission occurs are different from those for nonprecursor bursts. A modestly significant correlation is observed between the duration of the precursor emission and the duration of the main episode emission. Otherwise, no significant correlations were found between precursor and main episode emission characteristics. No unexpected significant correlations were found among either the precursor or main episode emission characteristics. No physically meaningful significant correlations were found between the separation time between events and any of the precursor or main episode emission characteristics.

In conclusion, we find no substantial evidence that the characteristics of the main episode emission are dependent upon the existence of the precursor emission, nor do we find any substantial indication that the precursor emission and main episode emission are the results of different burst environments or production mechanisms.

We wish to acknowledge Gordon Emslie, John Horack, Robert Mallozzi, and the anonymous referee for comments that were useful in improving this text.

REFERENCES

Briggs, M. S. 1993, ApJ, 407, 126
Brock, M. N., et al. 1992, in AIP Conf. Proc. 265, Huntsville Gamma-Ray Burst Workshop, ed. W. S. Paciesas & G. J. Fishman (New York: AIP), 383
Fishman, G. J., et al. 1989, in Proc. of the GRO Science Workshop, ed. W. N. Johnson (Greenbelt: NASA/GSFC), 2-39
Fishman, G. J., et al. 1994, ApJS, 92, 229
Harmon, B. A., et al. 1991, in Proc. Compton Obs. Science Workshop, ed. C. Shrader, N. Gehrels, & B. Dennis (NASA Conf. Publ. 3137) (Washington: NASA), 69
Hoffman, J. A., Marshall, H. L., & Lewin, W. H. G. 1978, Nature, 271, 630
Horack, J. M., et al. 1994, ApJ, 429, 319
Horack, J. M., & Emslie, A. G. 1994, ApJ, 425, 776
Kouveliotou, C., et al. 1993, ApJ, 413, L101
Lewin, W. H. G., van Paradijs, J., & Taam, R. E. 1993, Space Sci. Rev., 62, 233
Lochner, J. C. 1992, in AIP Conf. Proc. 265, Huntsville Gamma-Ray Burst Workshop, ed. W. S. Paciesas & G. J. Fishman (New York: AIP), 289
Meegan, C. A., et al. 1994a, in AIP Conf. Proc. 307, Second Huntsville Gamma-Ray Burst Workshop, ed. G. J. Fishman, J. J. Brainerd, & K. Hurley (New York: AIP), 289
Meegan, C. A., et al. 1994b, electronic catalog available from grossc.gsfc.nasa.gov, username gronews, the "BATSE 2B Gamma-Ray Burst Catalog"
Murakami, T., et al. 1991, Nature, 350, 592
Murakami, T., et al. 1992, in AIP Conf. Proc. 265, Huntsville Gamma-Ray Burst Workshop, ed. W. S. Paciesas & G. J. Fishman (New York: AIP), 28
Press, W., Flannery, B., Teukolsky, S., & Vetterling, W. 1986, Numerical Recipes (Cambridge: Cambridge Univ. Press)
Schmidt, M. 1968, ApJ, 151, 393
Yoshida, A., & Murakami, T. 1994, in AIP Conf. Proc. 307; Second Huntsville Gamma-Ray Burst Workshop, ed. G. J. Fishman, J. J. Brainerd, & K. Hurley (New York: AIP), 333